CrossMark

A framework for parameterization of heterogeneous ocean convection

Mehmet Ilıcak [a,*], Alistair J. Adcroft [b], Sonya Legg [b]

[a] Uni Climate, Uni Research AS, and Bjerknes Centre for Climate Research, Allégaten 55, 5007 Bergen, Norway
[b] Atmospheric and Oceanic Sciences, Princeton University, Princeton, NJ 08540, USA

ABSTRACT

We propose a new framework for parameterization of ocean convection processes. The new framework is termed "patchy convection" since our aim is to represent the heterogeneity of mixing processes that take place within the horizontal scope of a grid cell. We focus on applying this new scheme to represent the effect of pre-conditioning for deep convection by subgrid scale eddy variability. The new parameterization separates the grid-cell into two regions of different stratification, applies convective mixing separately to each region, and then recombines the density profile to produce the grid-cell mean density profile. The scheme depends on two parameters: the areal fraction of the vertically-mixed region within the horizontal grid cell, and the density difference between the mean and the unstratified profiles at the surface. We parameterize this density difference in terms of an unresolved eddy kinetic energy. We illustrate the patchy parameterization using a 1D idealized convection case before evaluating the scheme in two different global ocean-ice simulations with prescribed atmospheric forcing; (i) diagnosed eddy velocity field applied only in the Labrador Sea (ii) diagnosed global eddy velocity field. The global simulation results indicate that the patchy convection scheme improves the warm biases in the deep Atlantic Ocean and Southern Ocean. This proof-of-concept study is a first step in developing the patchy parameterization scheme, which will be extended in future to use a prognostic eddy field as well as to parameterize convection due to under-ice brine rejection.

© 2014 Elsevier Ltd. All rights reserved.

1. Introduction

Open ocean convection is one of the important sources of deep and intermediate waters which supply the downwelling branch of the meridional overturning circulation (MOC). The strength of the MOC, and hence the oceanic component of meridional heat transport, may be sensitive to the rate at which deep water is formed through surface cooling in subpolar seas (Dickson et al., 1990). A significant fraction of North Atlantic Deep water (NADW) is formed through convection in the Labrador Sea, where observations show water-mass formation rates of between 2–3 Sv (Sv≡ 10^{-6} m³/s) in years of weak forcing and 12 Sv in years of intense atmospheric forcing (Rhein and Coauthors., 2002; Smethie et al., 2001). Recent observations show that open ocean convection in the Irminger Sea also contributes to NADW (Våge et al., 2008; Våge et al., 2011). Open ocean convection in marginal seas (e.g. the Mediterranean, (Schott et al., 1991)) contributes to several different Atlantic water masses. (See Marshall and Schott, 1999 for a detailed review of open ocean convection.)

Buoyancy-driven ocean convective processes occur on very small time and spatial scales. The vertical water column can be mixed over hundreds of meters during a period of hours (Aagaard et al., 1989). Because of their small scales, these convection processes cannot be resolved in coarse resolution ocean general circulation models (OGCMs) typically used in climate studies, and have to be parameterized. Existing OGCMs employ different types of one-dimensional convective parameterizations, including convective adjustment schemes (Cox, 1984; Rahmstorf, 1993), enhanced diffusivities (Klinger et al., 1996) and penetrative mixed layer schemes (Large et al., 1994; Paluszkiewicz et al., 1997). These 1D parameterizations attempt to represent the vertical redistribution of water properties caused by buoyancy-loss induced rapid mixing. One source of error of these boundary layer parameterizations is that they are applied over the entire horizontal grid cell. This use of grid-cell wide parameterizations leads to homogenization of the water column over the entire $O(100 \times 100)$ km area, whereas in the real ocean convection mixes on much smaller scales, set by variations in stratification due to pre-existing ocean eddies, or variations in surface fluxes, leaving adjacent regions with finite stratification. As a result, the coarse model convection region will have smaller area-averaged stratification than the real ocean, given the same buoyancy loss.

---

* Corresponding author.
  E-mail address: mehmet.ilicak@uni.no (M. Ilıcak).
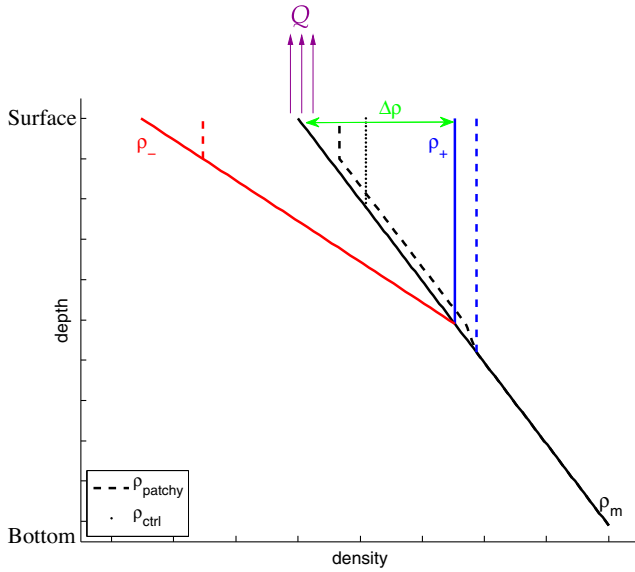
Fig. 1. Schematic of the patchy convection scheme. ρ_m (black solid) is the mean density profile (averaged over a grid-cell), ρ_+ (blue solid) is the convection-favorable constituent density profile, ρ_- (red solid) is the more stably-stratified constituent density profile. Blue and red dashed lines show the evolution of ρ_+ and ρ_- after convective mixing. Black dotted line shows the evolution of ρ_m after mixing with standard grid-cell-wide convection scheme; black dashed line shows the area-weighted sum of ρ_+ and ρ_- after mixing. (For interpretation of the references to color in this figure legend, the reader is referred to the web version of this article.)

Observational and numerical studies have shown eddy-restratification processes to be important in the Labrador Sea (Gelderloos et al., 2011; Jones et al., 1997). Lateral eddy fluxes bring buoyant water into the interior of the Labrador Sea (Lilly et al., 2003; Spall, 2004; Katsman et al., 2004), and dense convected water is exported out of the Labrador Sea into the boundary current (Straneo, 2006). There are ongoing efforts to parameterize the restratification of the mixed layer, based on the horizontal density gradient and the mixed layer depth (Boccaletti et al., 2007; Fox-Kemper et al., 2008).

In addition to restratifying the convection region in the Labrador Sea, eddies generated by the boundary currents are an important source of heterogeneity in the density field prior to the onset of convection (Lilly et al., 2002). The buoyant core of Irminger current anticyclones reduces the depth of mixing due to winter-time convection (Rykova et al., 2009). Numerical studies demonstrate that the presence of pre-existing eddies, by modifying the distribution of stratification, can alter the depth to which surface heat flux penetrates, and the eventual average stratification (Legg et al., 1998). Eddies also influence the pre-conditioning for convection in the Western Mediterranean (Demirov et al., 2007) and Greenland Seas (Gascard et al., 2002). A related problem of sub-grid-scale heterogeneity occurs under sea-ice, where leads give rise to patchy surface heat loss (Smith et al., 1990).

The effect of heterogeneous convection, due to pre-existing eddies or fragmented sea-ice has not yet been parameterized in GCMs. Steps in that direction include Campin et al. (2011), who proposed "super" parameterization to increase the stratification in the coarse OGCMs, where high resolution 2D non-hydrostatic models are embedded at each vertical column of a coarse resolution model, and Nguyen et al. (2009) who proposed a parameterization of brine rejection under ice, similar to the buoyancy loss due to cooling in ice-free regions, to increase the stratification in the Arctic Ocean and preserve the cold halocline. Losch et al. (2006) show that the inability of coarse resolution models to resolve heterogeneous mixing can introduce biases in the mixed layer depth and structure.

In this study, we propose a new conceptual framework to parameterize heterogeneous convective mixing in a coarse resolution ocean model. We have focused on the application of this new scheme to represent the effect of pre-conditioning for deep convection by sub-grid scale eddy variability in the density field. However, the parameterization can be also used to represent other heterogeneous mixing processes such as convection under sea ice. While the scheme makes no distinction between deep and shallow regions of the ocean, the parameterization is expected to have most impact in areas where the depth of convection is limited by variations in stratification, which is not usually the case for convection on coastal shelves. In the next section, we describe details of the parameterization and the physical parameters which are used for the test cases. In Section 3, the results of a 1D single column test case, and two different global model simulations are described. Finally, we summarize and conclude in Section 4, including suggestions for future work.

2. Patchy convection parameterization

We refer to the new parameterization as patchy convection since our aim is to represent the mixing processes which take place in only part of the horizontal grid cell rather than over the full cell. Details of patchy convection are the following. We assume that a fraction, A, of the horizontal area of a coarse numerical ocean grid cell is favorable to deep convection, where $0 \leqslant A \leqslant 1$, and the rest of the grid cell $(1 - A)$ is more strongly stratified. Coarse resolution climate models represent the grid-cell mean density profile, averaged over these two different areas. We separate the grid-cell mean density profile (ρ_m in Fig. 1)) into two different component profiles; one, applied over fraction A, is unstratified and favorable
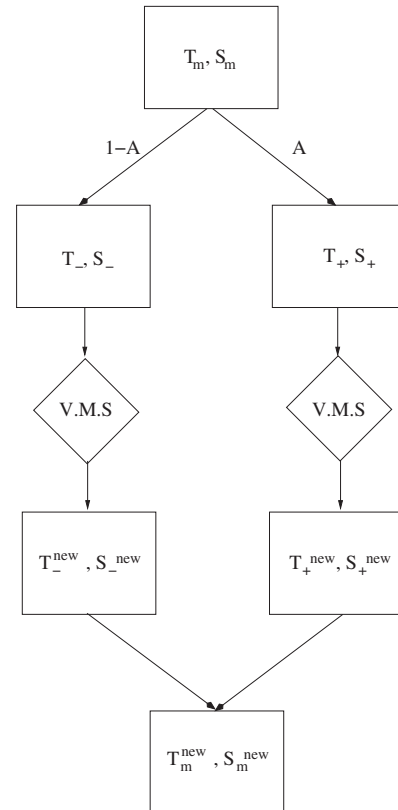
Fig. 2. Algorithm of the patchy convection scheme. Decompose the mean variables (T_m, S_m) into two profiles. Apply any type of vertical mixing scheme (V.M.S) to the new profiles to get $(T_-^{new}, S_-^{new}, T_+^{new}, S_+^{new})$. Combine the decomposed values to obtain new mean profiles.

to convection, and therefore denser near the surface (ρ_+, blue line in Fig. 1) and the other one, applied over fraction $1 - A$, is more strongly stratified, i.e. less dense near the surface, and less favorable to convection (ρ_-, red line in Fig. 1). The coarse resolution ocean model mean profile can therefore be decomposed as

$$\rho_m = A\rho_+ + (1 - A)\rho_-. \qquad (1)$$

When a buoyancy forcing, Q, is applied over the whole grid-cell to the mean profile (the control case), it will mix vertically from the surface. The resulting profile after cooling is shown as the black dotted line in Fig. 1. Depending on which convection scheme is used, there might be a penetrative region at the bottom of the mixed layer; however for simplicity we ignore this (i.e. assuming standard convective adjustment). Alternatively, if Q is applied separately to the two component profiles ρ_+ and ρ_-, they will mix differently and will lead to different vertical structures. The convection-favorable profile ρ_+ will mix the cold water deeper into the ocean (blue dashed line in Fig. 1) and the strongly stratified profile ρ_- will have shallow mixing (red dashed line in Fig. 1). When we sum up the two profiles using the area ratios, the vertical stratification of the averaged profile is increased relative to that in the control profile (see black dashed and dotted lines in Fig. 1) and cold water penetrates more deeply than the control case.

There are only two parameters needed to close this patchy convection scheme; area fraction, A, and the density difference between the unstratified profile and the mean profile, $\Delta\rho = \rho_+ - \rho_m$ at the surface. The parameter $\Delta\rho$ represents the amplitude of mesoscale density perturbations due to pre-existing eddies, generated by baroclinic instability of the large-scale currents, e.g. the boundary currents in the Labrador Sea. To specify $\Delta\rho$, we will use the following scaling to relate it to eddy kinetic energy, EKE, which will be an external input to the parameterization. If we assume individual eddy structures are in thermal wind balance:

$$\frac{\partial u}{\partial z} \cong \frac{g}{f\rho_0} \frac{\partial \rho}{\partial y}, \qquad (2)$$

(where f is the Coriolis parameter, g is the acceleration due to gravity and ρ_0 is the mean density, $\partial u/\partial z$ is the vertical shear of the azimuthal current, and $\partial \rho/\partial y$ is the radial density gradient), we can integrate over the lateral scale of the eddy, L_c, and vertical scale, H, to yield a relation between density difference, $\Delta\rho$ and eddy velocity scale, U_e:

$$\frac{U_e}{H} \sim \frac{g}{f\rho_0} \frac{\Delta\rho}{L_c}. \qquad (3)$$

The mesoscale eddy velocity can be expressed in terms of EKE as $U_e = \sqrt{2EKE}$, and hence we obtain a scaling for $\Delta\rho$ in terms of EKE

$$\rho_+ - \rho_m = \Delta\rho = \frac{\gamma\sqrt{EKE}L_c f\rho_0}{gH} \qquad (4)$$
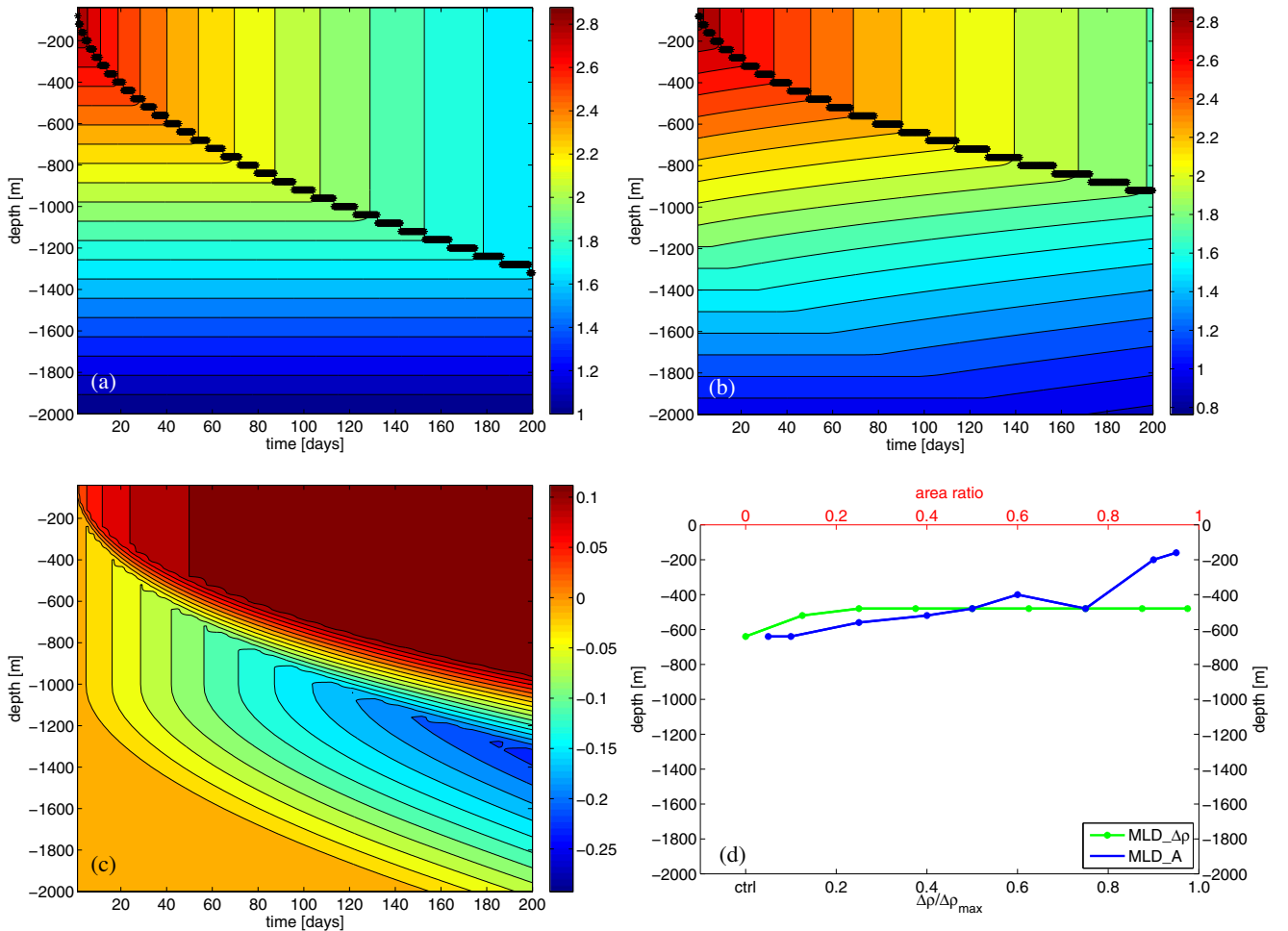
Fig. 3. (a) Temperature profile vs. time for the single column control case; black dots indicate the mixed layer depth in time; (b) Temperature profile vs. time for the single column patchy case with $\Delta\rho = 0.2$ and $Area = 0.5$; black dots indicate the mixed layer depth in time (c) Temperature difference between patchy convection and control case vs. time; (d) Mixed layer depths at a time = 50 days, as a function of density difference $\Delta\rho$ and area ratio A: MLD_$\Delta\rho$ for variable $\Delta\rho$ (green), MLD_A for variable A (blue). (For interpretation of the references to color in this figure legend, the reader is referred to the web version of this article.)
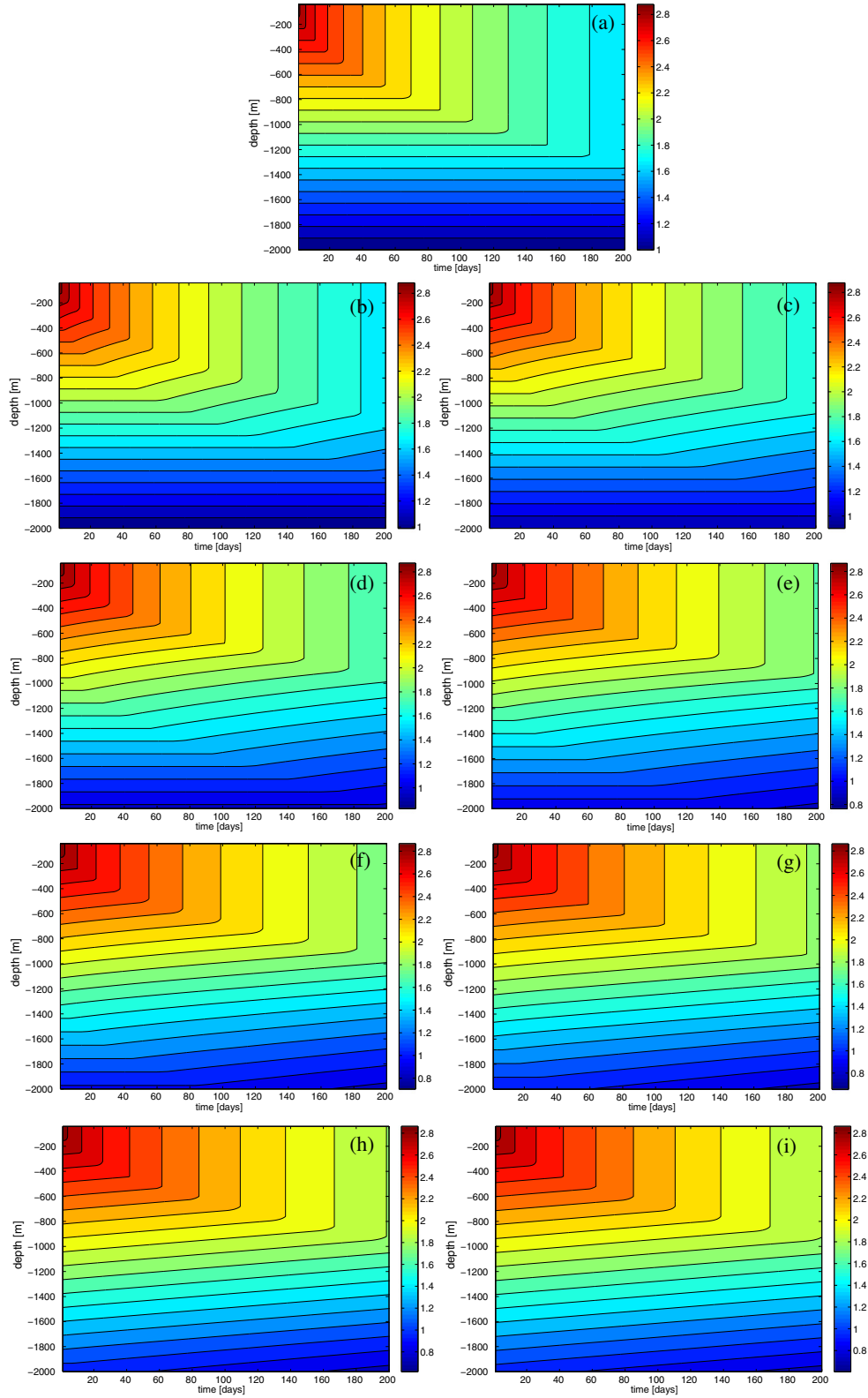
Fig. 4. (a) Temperature profile vs. time for the single column control case; Temperature profile vs. time for the patchy convection case where (b) $\Delta\rho/\Delta\rho_{max} = 0.125; Area = 0.5$; (c) $\Delta\rho/\Delta\rho_{max} = 0.25; Area = 0.5$; (d) $\Delta\rho/\Delta\rho_{max} = 0.4; Area = 0.5$; (e) $\Delta\rho/\Delta\rho_{max} = 0.5; Area = 0.5$; (f) $\Delta\rho/\Delta\rho_{max} = 0.625; Area = 0.5$; (g) $\Delta\rho/\Delta\rho_{max} = 0.75; Area = 0.5$; (h) $\Delta\rho/\Delta\rho_{max} = 0.875; Area = 0.5$; (i) $\Delta\rho/\Delta\rho_{max} = 0.975; Area = 0.5$.

where we have introduced a tunable nondimensional coefficient, γ, which represents the uncertainties in the various scaling assumptions. For example, we have used the column depth (i.e.

the ocean depth) for the vertical scale, H, in the above scaling on the assumption that the main contributions to *EKE* are from the gravest mode eddies. The vertical scale of these eddies is
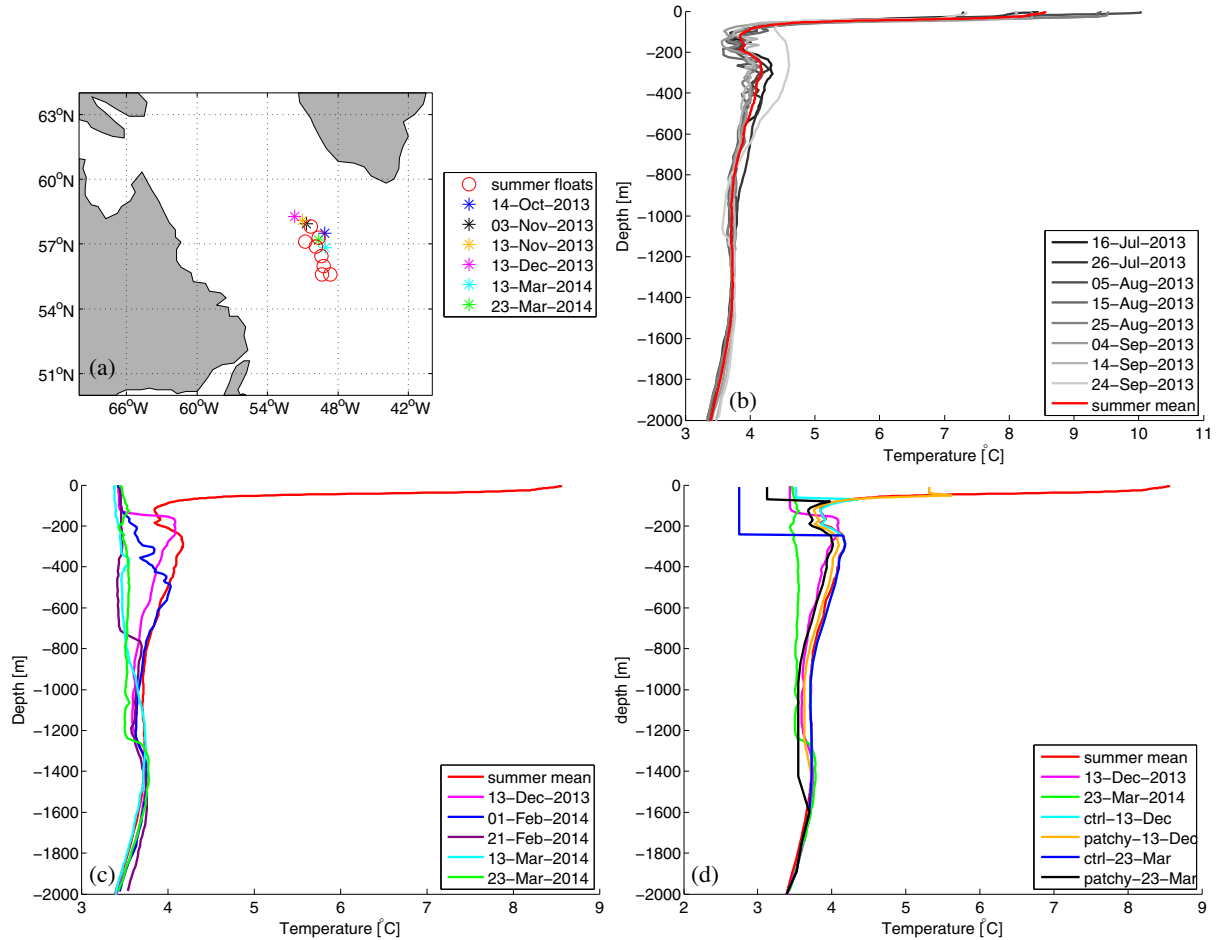
Fig. 5. (a) Locations of some of the Argo floats, red circles (summer floats) are used to compute initial stratification. (b) Temperature profiles of the summer time floats. The red profile is the ensemble mean of the summer floats. (c) Temperature profiles of the winter floats. (d) Temperature profiles of the control case and patchy scheme at days 74 and 174. (For interpretation of the references to color in this figure legend, the reader is referred to the web version of this article.)

generally some fraction of the column depth which we absorb into the nondimensional parameter, γ. The sensitivity of results to γ will be discussed later. The characteristic length scale is defined as the minimum of the Rossby radius of deformation, R_d, or the numerical model grid scale (i.e. $L_c = min[R_d; \Delta x]$), ensuring that the patchy convection will be turned off in high resolution simulations (i.e. when $\Delta x \ll R_d$). Since resolution dependence is introduced in the $\Delta \rho$ length scale, there is no need for resolution dependence in A. (Alternatively A could be set to zero when $\Delta x < R_d$). In this study, R_d is computed using the first baroclinic Rossby radius of deformation employing the WKB approach described by Chelton et al. (1998). The patchy convection algorithm (Fig. 2) is therefore as follows:

- Calculate $\Delta \rho$, (the density difference at the surface), from Eq. (4) and hence determine the depth over which the density profile is separated into an unstratified component and a more strongly stratified component – i.e. the depth d at which $\rho_m(z) = \rho_+$ (See Fig. 1).
- T_+ and S_+, the temperature and salinity which contribute to that density are set to be the values at depth d, and like ρ_+ are unstratified in the upper ocean.

- T_- and S_-, the temperature and salinity profiles corresponding to the more strongly stratified region are found from the difference between the mean profiles (T_m, S_m) and (T_+, S_+) using Eq. (1).

- Apply any type of vertical mixing scheme (V.M.S) such as convective adjustment, enhanced diffusivity, KPP (Large et al., 1994) or two-equation turbulence closures (Ilıcak et al., 2008) to obtain new profiles.
- Combine the new profiles (T_+^{new}, S_+^{new} and T_-^{new}, S_-^{new}) to obtain the mean profile using Eq. (1).

3. Results

We conducted a hierarchy of experiments. Idealized 1D vertical column simulations demonstrate the patchy convection scheme and explore the sensitivity to the parameters A and $\Delta \rho$. To compare the scheme against observations, we employed the 1D case using the summer time ARGO floats from the Labrador Sea as initial conditions. We used ECMWF reanalysis atmospheric forcing and compared our results to the winter time ARGO floats. A global ocean-ice simulation using CORE-I nominal year forcing (Griffies et al., 2009) acts as a control experiment (brief details of that experiment can be found in Section 3.2), which is compared with global CORE-I forced ocean-ice simulations employing the new parameterization scheme. The eddy velocity scale was estimated from a balance between APE extraction by the Gent–McWilliams parameterization and a local bottom drag with a spin-down time-scale of 100 days (Cessi, 2008, Eq. (4)) using fully coupled simulations using climate model CM2M (Dunne et al., 2012), and imposed as a static map. A first group of simulations imposes the

eddy field only in the Labrador sea region, in order to calibrate other parameters such as γ. Finally, in Section 3.3 the eddy velocity field is prescribed globally.

3.1. 1D vertical convection test case

Here, we demonstrate the effect of the patchy convection framework in an idealized experiment. The modular ocean model (MOM) (Griffies, 2012) is used as a one dimensional columnar test case. The total water depth is 2000 m and the initial temperature profile decreases uniformly from 3 °C at the surface to 1 °C at the bottom. We used uniform salinity which is 35 psu and applied uniform cooling, $Q = -200$ W/m^2, for 200 days. A linear equation of state is used to compute density for this idealized experiment. The maximum density difference between the top and bottom of the ocean is $\Delta\rho_{max} = 0.4$ kg/m^3. We employed both the convective adjustment scheme described by Rahmstorf (1993) and the KPP scheme as the vertical mixing schemes for all experiments. The two vertical mixing schemes give qualitatively similar results, so we focus on the convective adjustment cases. There are a total of 17 experiments: the control simulation (no patchy convection); 8 different experiments changing $\Delta\rho$ values (0.05, 0.1, 0.15, 0.2,

0.25, 0.3, 0.35, 0.39) while keeping area ratio A constant at 0.5; and an additional 8 experiments changing area ratio values ($A = 0.05$, 0.1, 0.25, 0.4, 0.6, 0.75, 0.9, 0.95) while keeping $\Delta\rho$ constant at 0.2 kg/m^3. These values of $\Delta\rho$ and A are intended to cover all possibilities, as well as extremes we do not expect to find in the real ocean, in order to test the full range of behavior of the scheme.

The temperature profile as a function of time for the control case is shown in Fig. 3(a). The cooling leads to vertical homogenization and the mixed layer depth deepens from 200 m to 1300 m in 200 days. The temperature field of the patchy case ($\Delta\rho = 0.2$ and $A = 0.5$) and the temperature difference between the patchy convection case and control case can be seen in Fig. 3(b) and (c), respectively. Cold water reaches deeper in the patchy convection case and the stratification in the patchy convection scheme case is larger (more warm water at the upper ocean and more cold water in the deeper part) than the stratification in the control case at the end of day 200. These results are consistent with simulations of deep ocean convection performed by Legg et al. (1998) with and without eddy heterogeneity in the initial temperature field. The mixed layer depth (MLD) as a function of time is plotted in the Fig. 3(a) and (b) (black dots). We defined the MLD as the depth where $\partial T/\partial z$ changes sign. The mixed layer depths at time = 50 days as a function of density difference and area fraction are shown in Fig. 3(d). The evolution of temperature field for several values of density difference are also shown in Fig. 4. The density difference, $\Delta\rho$, is normalized by the maximum density difference $\Delta\rho_{max}$. MLD stays constant increasing $\Delta\rho$ in the patchy convection scheme (green line). There is a slight decrease in MLD2 when we change the area (blue line in Fig. 3(d)). In view of this relative insensitivity to the area fraction, we decided to use a constant area fraction of $A = 0.5$ in all further numerical experiments. Thus, we assume half of the grid-cell is favorable to convection, and therefore assume the mean profile in the OGCMs can be represented by two equally weighted profiles. Higher values of area fraction lead to more cold water at depth compared to the control case (not shown).

Next, we conducted two additional experiments using the ARGO floats obtained from the Labrador Sea during summer and winter 2013. The locations of the ARGO floats are shown in Fig. 5(a). These data were collected and made freely available by the Coriolis project and programmes that contribute to it (http://www.coriolis.eu.org). The temperature profiles of the summer floats as a function of depth are shown in Fig. 5(b). We took the mean of the profiles obtained between 16 August 2013 and 24 September 2013 (red line in the same figure) and used both mean temperature and salinity (not shown here) profiles as our initial conditions for the 1D model. Then we forced the idealized model using the atmospheric forcing acquired from the ECMWF reanalysis data between 1st October 2013 and 30th March 2014. Fig. 5(c) shows the temperature profiles of the ARGO floats during the same time period. Atmospheric cooling generates a vertically mixed layer depth down to 200 m by December 2013. The December ARGO float also shows cooling at depth, below the mixed layer (magenta line vs. red line). Later in the winter, the mixed layer deepens and the vertical column is well mixed down to 1200 m by the end of the March 2013.

We ran two concurrent simulations with and without patchy convection scheme using a nonlinear equation of state, the area ratio 0.5 and density difference 1.007 kg/m^3. The application of the new parameterization is independent of choice of equation of state. Using Eq. (4), we compute the depth where the in situ density difference from the surface is larger than $\Delta\rho$. Then, we use that depth to apply the patchy scheme separately to the temperature and salinity profiles. The density (and therefore equation of state) is only used to find the depth above which we do the decomposition. The decomposition is otherwise independent of the equation of state and conserves T and S correctly.
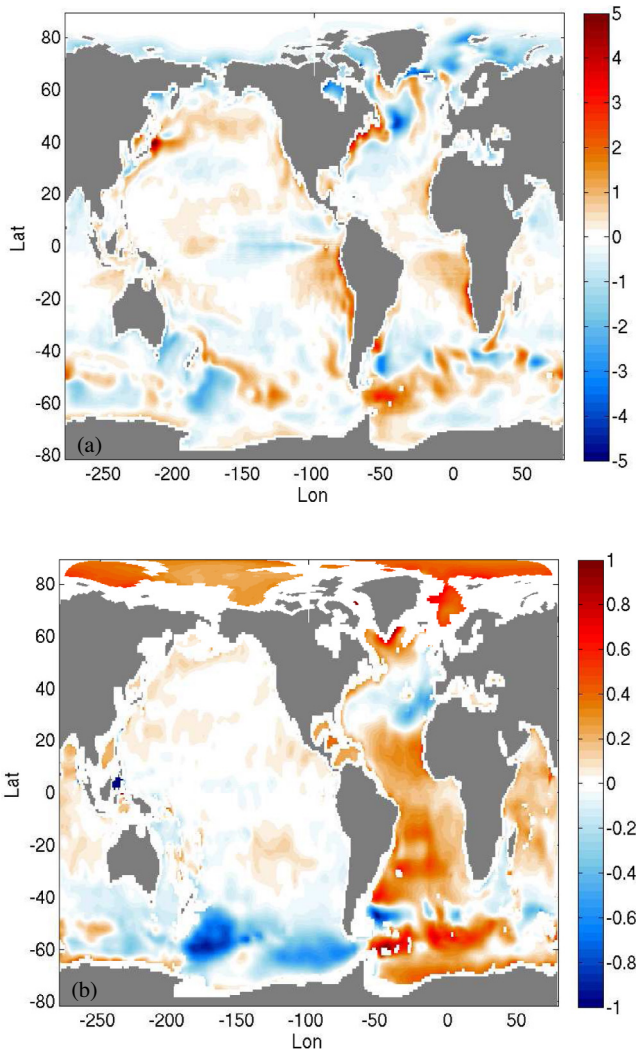
Fig. 6. Temperature bias (degrees C) for years 100–200 years of the nominal year forcing control case from World Ocean Atlas climatology at (a) z = 5 m and (b) z = 2000 m.
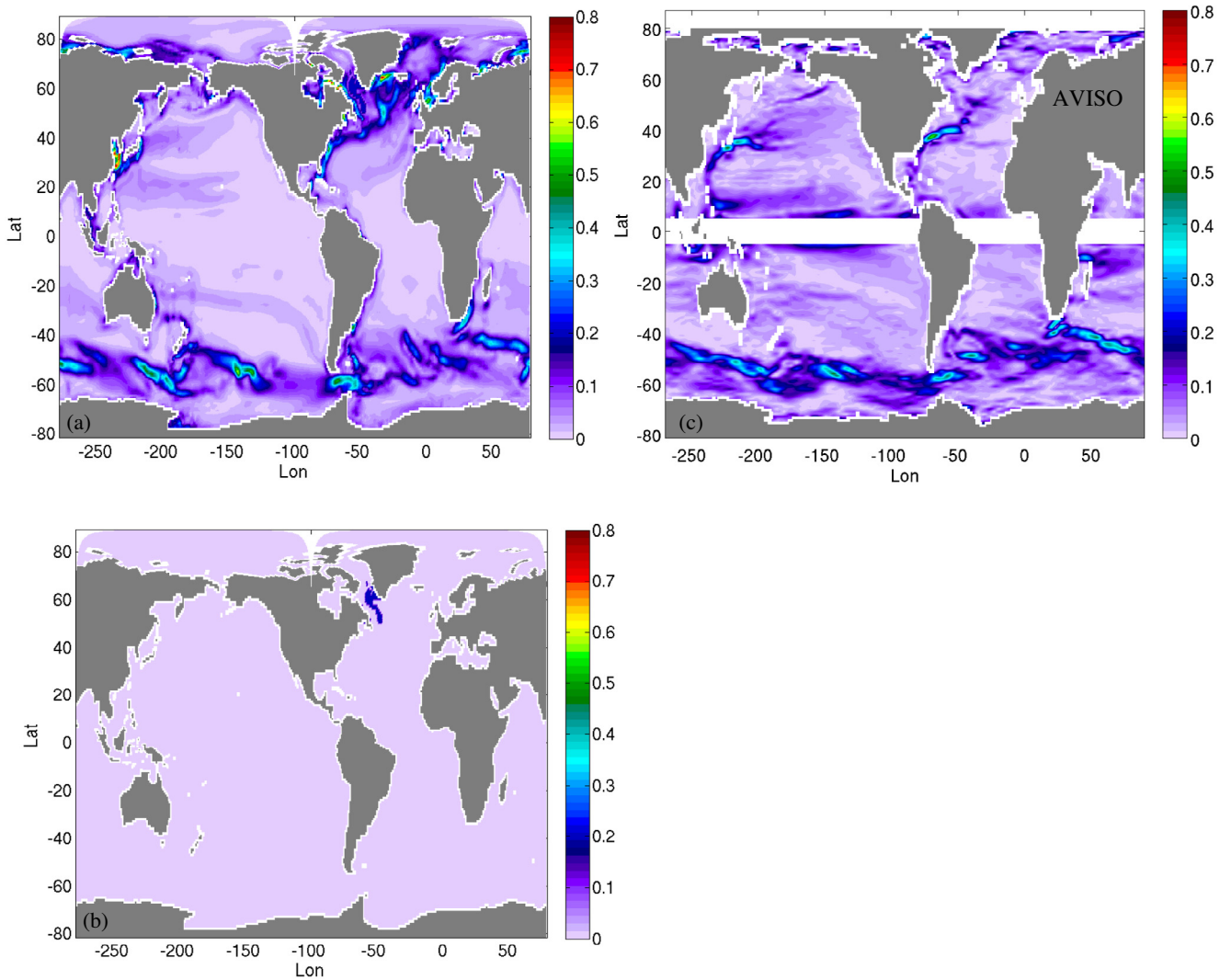
Fig. 7. (a) Eddy velocity field in m/s of the global experiment (b) Eddy velocity field in m/s of the Labrador Sea eddy field experiment. (c) Mean eddy velocities from AVISO satellite data (http://podaac.jpl.nasa.gov/dataset/AVISO_L4_DYN_TOPO_1DEG_1MO).

Fig. 5(d) shows the temperature profiles of the control case and patchy simulations at 13th December 2013 and 23th March 2014. In the control case, the upper ocean (75 m and above) cooling was comparable to the observations on December 13. However the control simulation was much warmer in the deep ocean (cyan line). On the other hand, the patchy scheme was more successful in exporting cold water into the deep ocean. However, the surface mixed layer is relatively warmer than the observations in the patchy case. In March 2014, the control simulation is colder (warmer) than the observations in the upper (deeper) ocean. The control simulation is 0.8 °C colder in the upper 250 m. The temperature profile in the patchy simulation is always colder than the control case between 150 m and 1300 m. In comparing the observed profiles with the 1D simulations, it is important to note that the vertical structure of the Labrador Sea is only sampled by a single float at each instant in this region, whereas the modeled results represent a horizontal average over a coarse-resolution grid cell. For a more rigorous test of the 1D scheme, we would need a larger number of simultaneous observations in the Labrador sea. Note also that we kept the $\Delta\rho$ constant throughout the six months integration time in our idealized 1D patchy simulation, which is another source of discrepancy. The density difference would change with time in global coupled simulations. Nevertheless, it is clear that while both control and patchy scheme simulations have difficulty reproducing the exact observed profile, the patchy scheme is an improvement, leading to greater cooling at depth, and increasing the stratification, as expected.

3.2. Global ocean-ice simulations with CORE-I forcing

As a control case for global simulations, an ocean-ice configuration of MOM4p1 is performed forced by normal year CORE forcing (Griffies et al., 2009). The ocean component uses the Arakawa B-grid with the same grid resolution and bathymetry as the CM2.1 ocean component documented by Griffies et al. (2005). The horizontal grid has a nominal 1° resolution (refined meridionally to 1/3° at the equator) and a tripolar grid poleward of 65°N. The vertical grid uses 50 levels, with 22 in the upper 220 m. All global simulations performed in this study use a non-linear equation of state. We use κ-profile parameterization (KPP) for diapycnal mixing proposed by Large et al. (1994). The model is integrated for 200 years. All the results are averaged between 100 and 200 years using a non-linear equation of state. The global map of sea surface temperature (SST) bias from the World Ocean Atlas climatology is shown in Fig. 6(a). The model exhibits a warm bias near the west coasts of the American and African continents in upwelling regions,
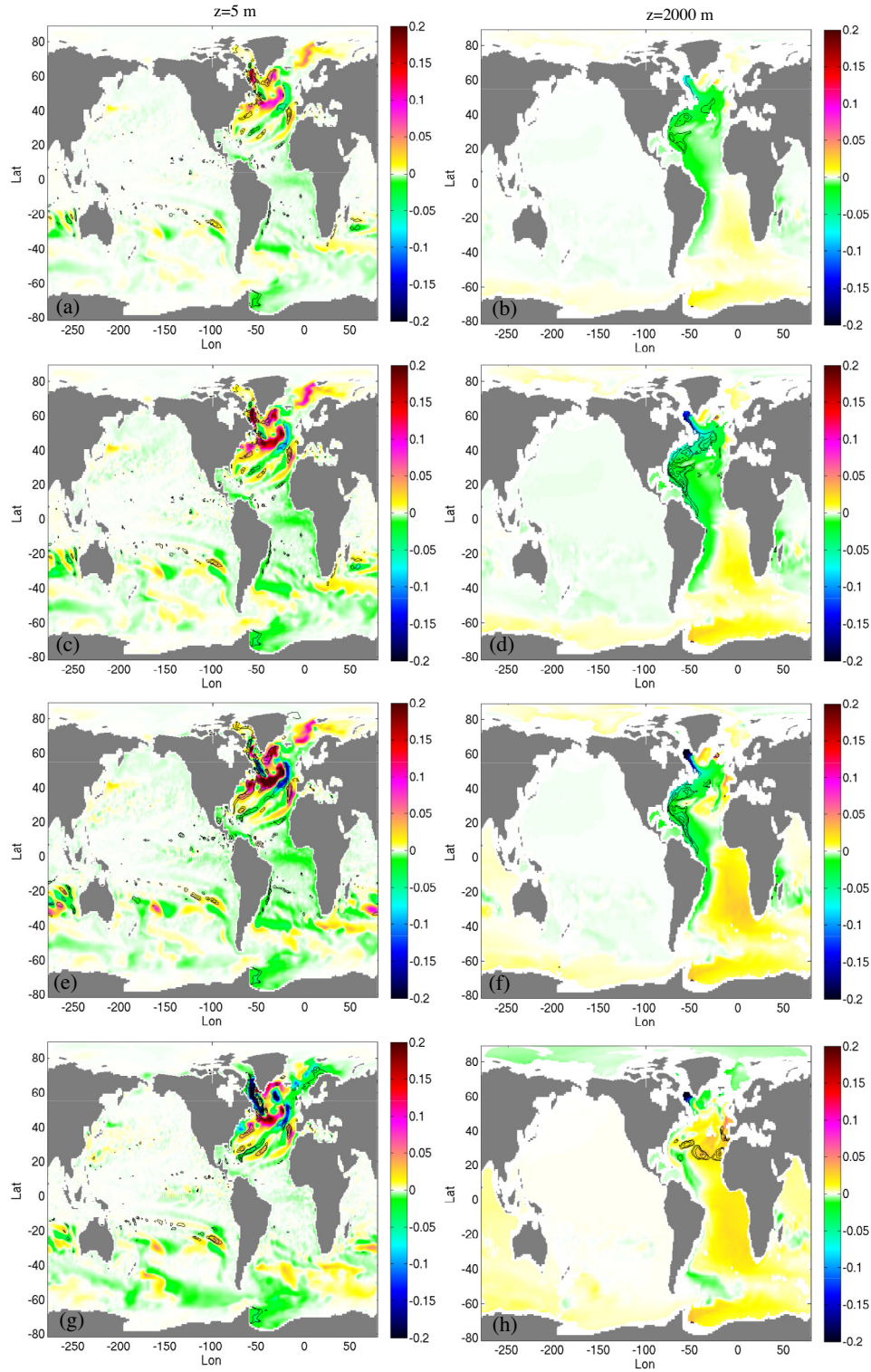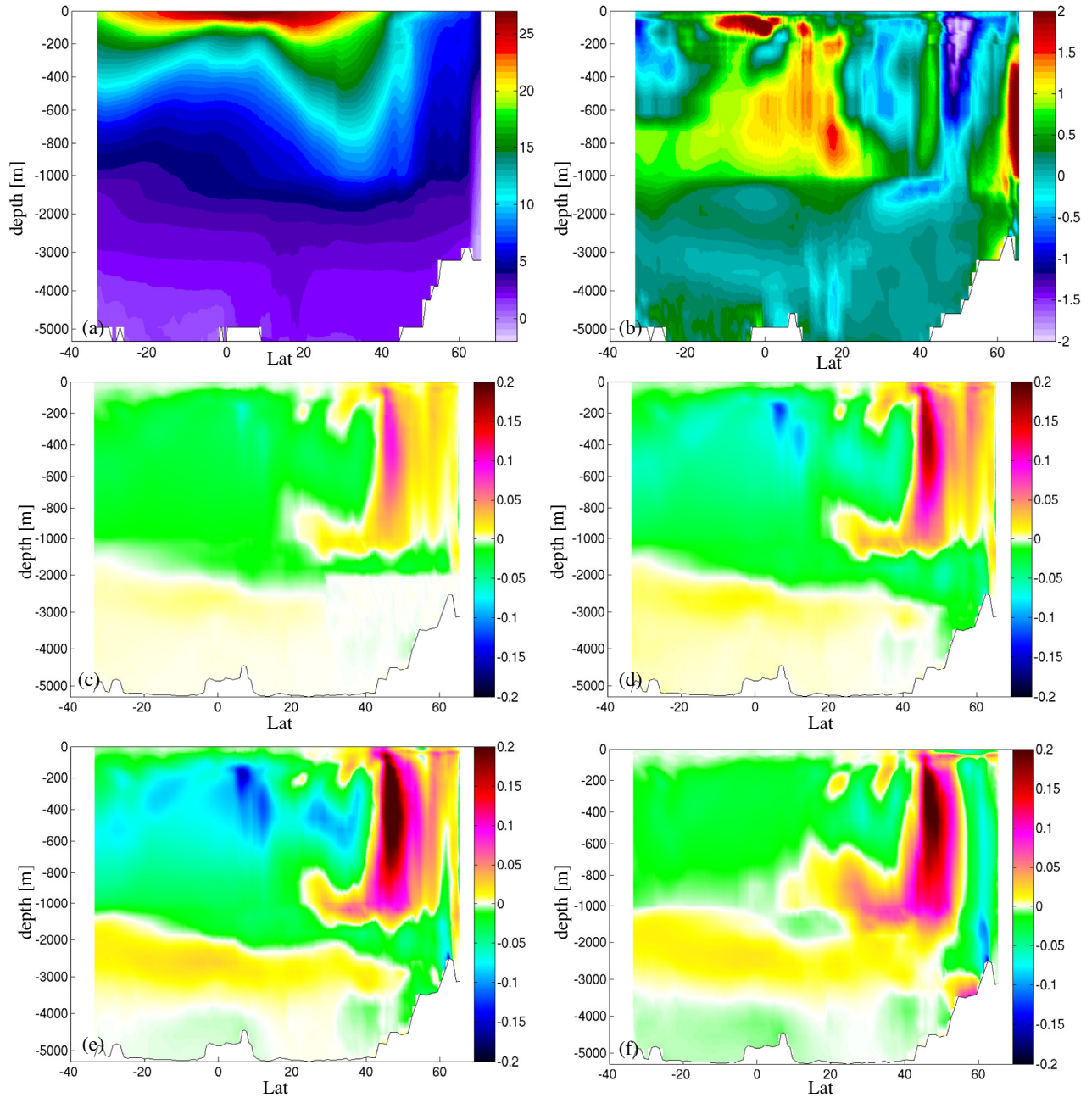
Fig. 8. (a) Horizontal section of the temperature difference between $\gamma = 0.15$ Labrador sea eddy field and control experiments at $z = 5$ m; (b) $z = 2000$ m; (c) same as (a) but for $\gamma = 0.5$; (d) same as (b) but for $\gamma = 0.5$; (e) same as (a) but for $\gamma = 1.25$; (f) same as (b) but for $\gamma = 1.25$; (g) same as (a) but for $\gamma = 5$; (h) same as (b) but for $\gamma = 5$.

probably due to coarse grid resolution and errors in the direction of near coastal winds (Griffies et al., 2009). There are also some large SST errors found along the Gulf Stream and Kuroshio currents in the North Atlantic and North Pacific, respectively. In the North Atlantic subpolar gyre region, the model shows signs of difficulties maintaining the North Atlantic drift (i.e. Gulf Stream) in the proper position, leading to a strong cold bias in the North Atlantic.

The temperature bias at 2000 m depth is shown in Fig. 6(b). The deep ocean is warmer than the climatological values especially in the Atlantic Ocean. The warm bias can be traced from the Labrador Sea and is advected along the western boundary current (see the movie in the additional items). These biases are consistent with inaccurate representation of convection processes in high latitudes including insufficient penetration of cold water to the deep ocean.

Fig. 9. (a) Vertical section of the zonally averaged temperature field of the control experiment in the Atlantic Ocean. (b) Vertical section of the zonally averaged temperature difference between control experiment and WOA climatology in the Atlantic Ocean. (c) Vertical section of the zonally averaged temperature difference between $\gamma = 0.15$ Labrador sea eddy field and control experiments in the Atlantic Ocean; (d) same as (c) but for $\gamma = 0.5$; (e) same as (c) but for $\gamma = 1.25$; (f) same as (c) but for $\gamma = 5$.

In order to use the patchy convection scheme, two variables are needed to compute the density difference between the mean and the unstratified profiles ($\Delta\rho$); the proportionality constant γ and the eddy velocity U_e. Models which do not resolve the heterogenous stratification due to eddies also do not resolve the velocity field due to eddies. However, the eddy velocity scale can be estimated from the Gent–McWilliams scheme used to parameterize mesoscale eddies in the coarse resolution model. We follow Eq. (4) of Cessi (2008) and assume a balance between APE extraction by the Gent–McWilliams parameterization and a local bottom drag with a spin-down timescale of 100 days to obtain U_e. To simplify analysis, the eddy velocity field was diagnosed from a control run and averaged over 5 years and applied in the patchy convection scheme as time-invariant, avoiding (for now) coupled

evolution of the hypothesized eddy velocity field and the patchy scheme. In order to diagnose the eddy velocity from a simulation in statistical equilibrium, we use a 2000 year global coupled climate simulation of CM2M (Dunne et al., 2012), which employs the same ocean model as used in our study. The eddy field from high resolution eddy-resolving simulations or from observations could also be used, but our intent in future is to use an eddy velocity field which evolves as the ocean state changes within a coarse resolution climate model simulation. We therefore prefer to explore the feasibility of using the GM-derived eddy velocity which can be diagnosed from within the coarse resolution model. However, we chose not to use the GM-derived velocities from the actual simulations in which we implement the patchy scheme since we want to first test the sensitivity to a static map of eddy velocities.
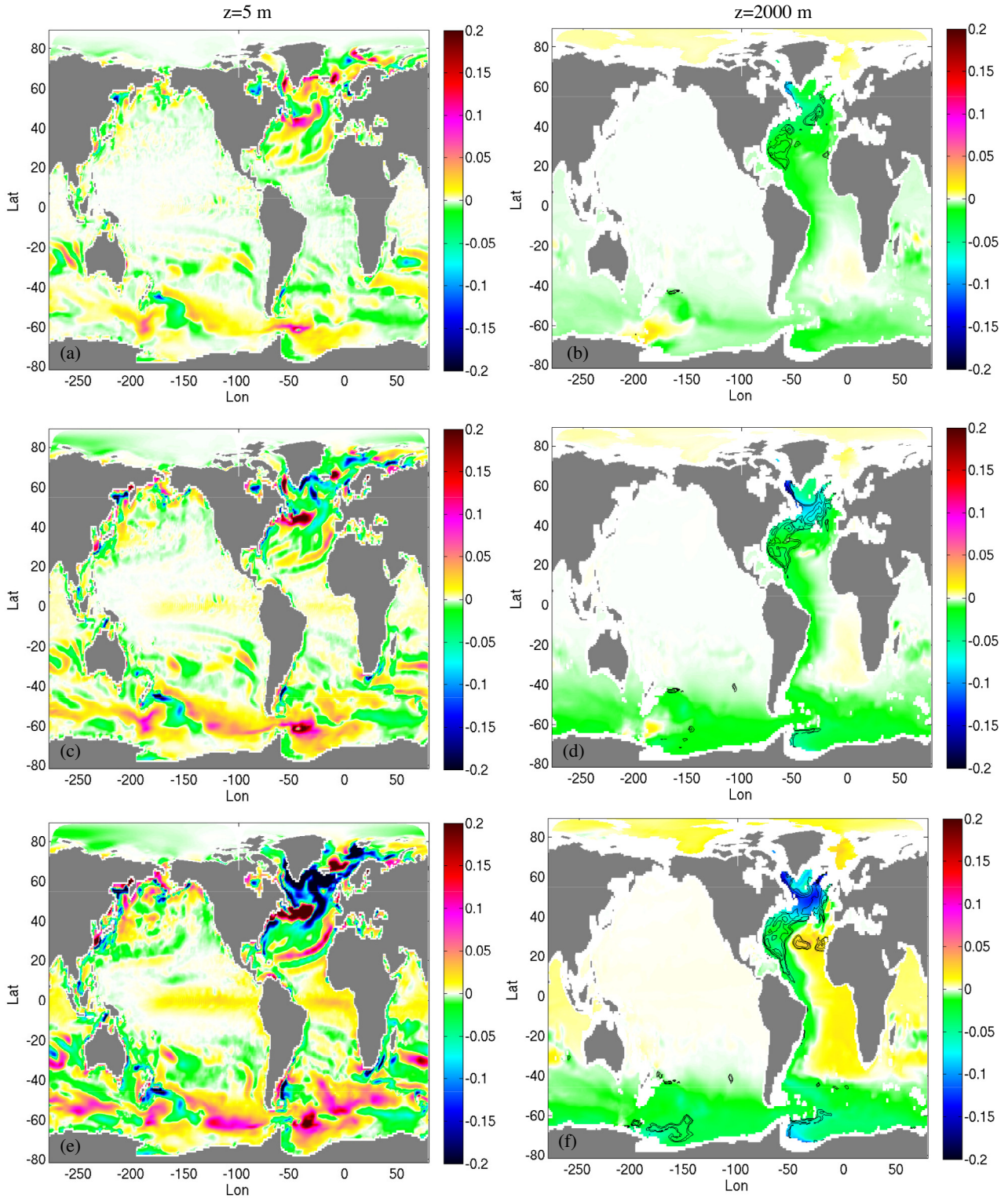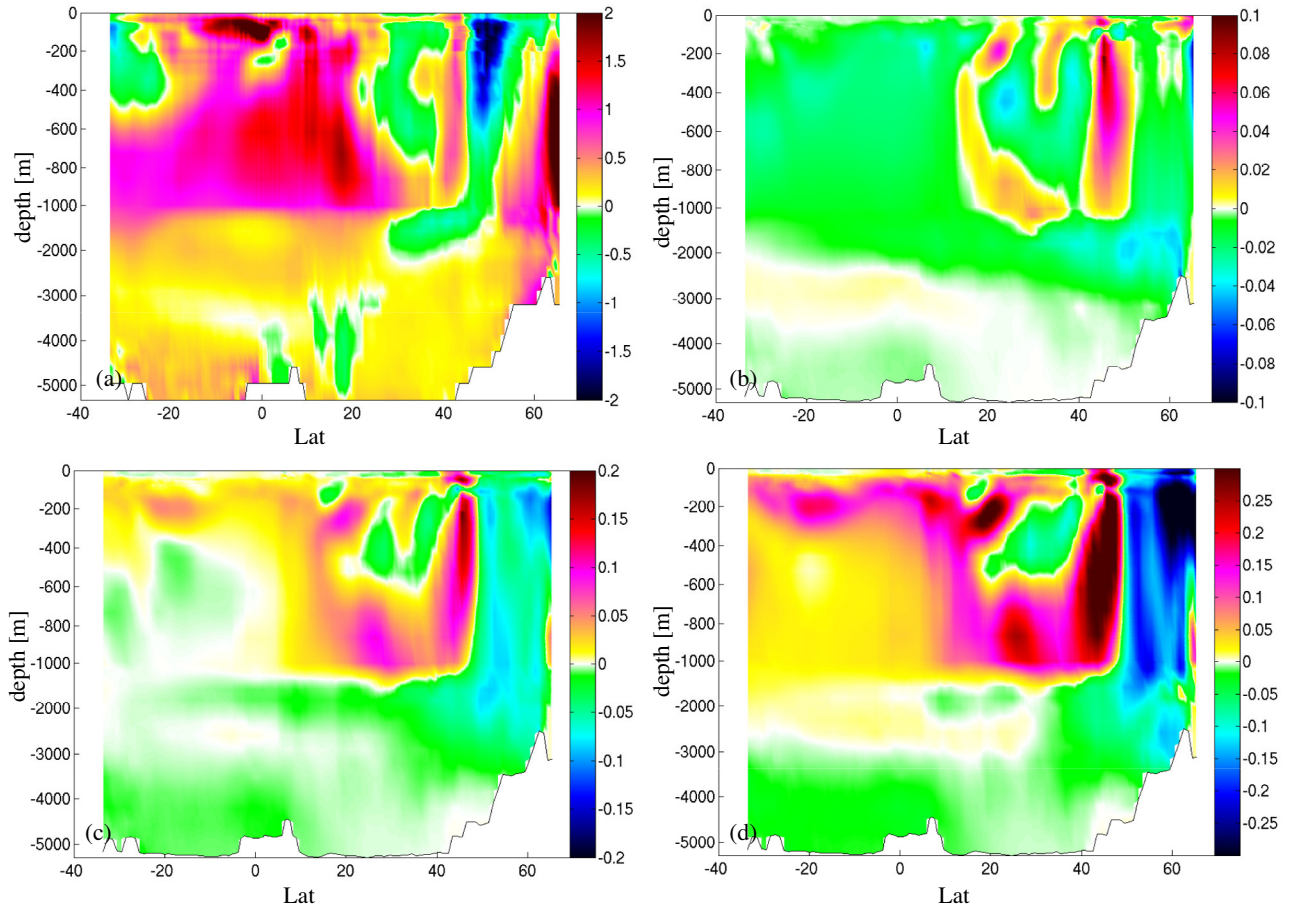
Fig. 10. (a) Horizontal section of the temperature difference between $\gamma = 0.15$ global eddy field and control experiments at $z = 5$ m; (b) Horizontal section of the temperature difference between $\gamma = 0.15$ and control experiments at $z = 2000$ m; (c) same as (a) but for $\gamma = 0.5$; (d) same as (b) but for $\gamma = 0.5$; (e) same as (a) but for $\gamma = 1.25$; (f) same as (b) but for $\gamma = 1.25$.

The eddy velocity field shown in Fig. 7(a) has a complex horizontal structure. The eddy velocities computed from the AVISO (Archiving, Validation and Interpretation of Satellite Oceanographic data) satellite data on a 1 degree grid are also shown in Fig. 7(c) for comparison. The dataset is obtained from http://pod-aac.jpl.nasa.gov/dataset/AVISO_L4_DYN_TOPO_1DEG_1MO. There

is a reasonable agreement between GM derived velocity values and AVISO values. Most of the eddy activity is in the Southern Ocean and western boundary currents such as the Gulf Stream. In addition the GM parameterization also yields high values of U_e at the eastern part of Greenland (a location where AVISO cannot resolve the small scale of the deformation radius). In order to iso-
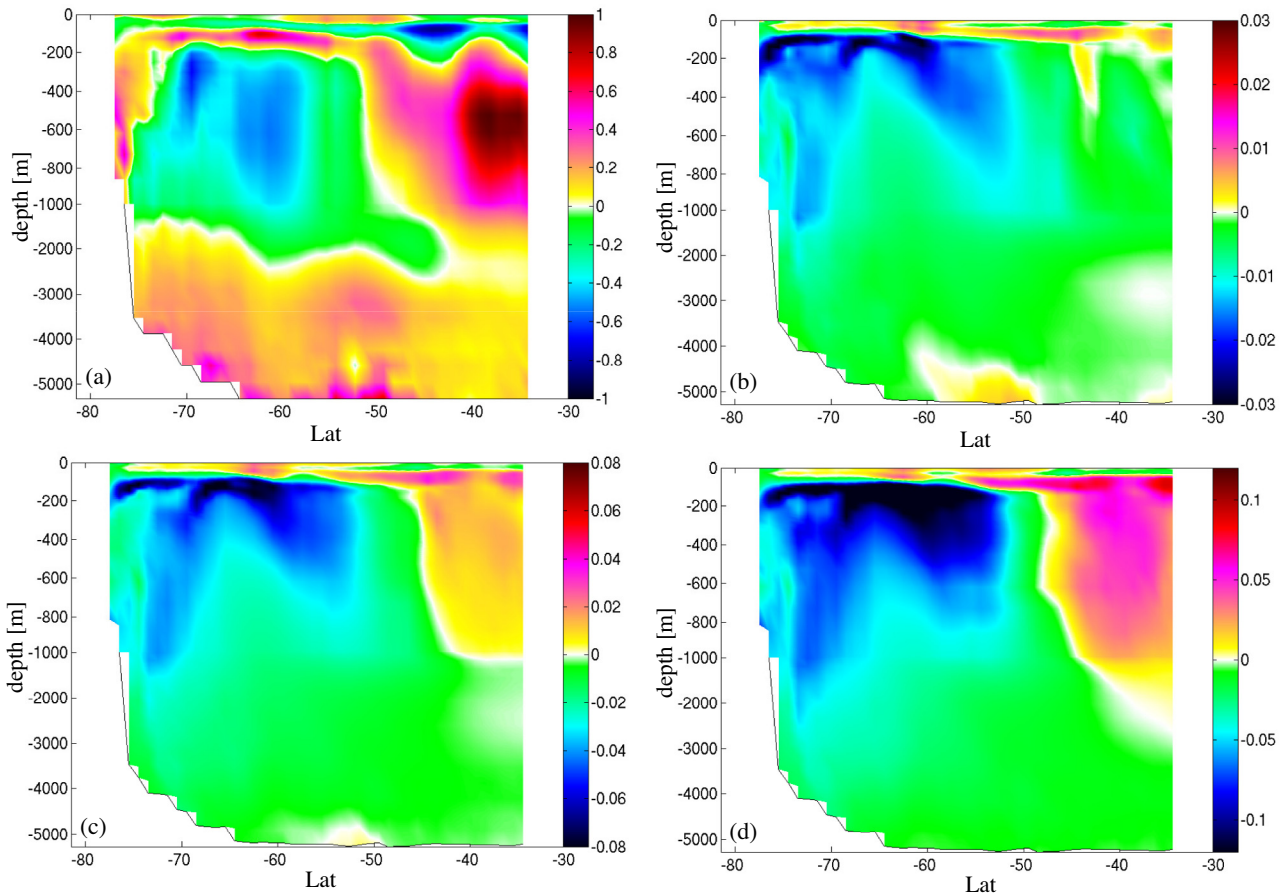
Fig. 11. (a) Vertical section of the zonally averaged temperature difference between control experiment and climatology in the Atlantic Ocean; (b) Vertical section of the zonally averaged temperature difference between $\gamma = 0.15$ global eddy field and control experiment in the Atlantic Ocean; (c) same as (b) but for $\gamma = 0.5$; (d) same as (b) but for $\gamma = 1.25$. Note that the colorbars are different.

late the effect of our new scheme in open ocean convection areas, we set the eddy velocity field to zero everywhere except the Labrador Sea region (Fig. 7(b)), ensuring that the patchy convection scheme will only be effective around the Labrador Sea. We conducted some sensitivity tests using four different γ values, 0.15 ,0.5, 1.25, and 5, which correspond to very weak ($\gamma = 0.15$), weak ($\gamma = 0.5$), moderate ($\gamma = 1.25$) and strong ($\gamma = 5$) proportionality factors, respectively. A smaller γ value corresponds to a smaller $\Delta\rho$. The area fraction used in the patchy parameterization is kept constant at 0.5 in all simulations.

100-year averaged sea surface temperature differences between different γ cases and the control simulation are provided in Fig. 8(a), (c), (e) and (g) for the Labrador Sea eddy field experiment. Although the new parameterization changes the convective parameterization only in the Labrador Sea region, there are distinct cold-warm anomalies on the surface over the whole Atlantic Ocean. The same type of wave pattern can also be found in the Southern Ocean. In order to determine whether the signal on the surface is important or not, a t-test is used. We used 10 year box-averaging to remove most Rossby wave signals. Confidence levels of 75% are shown by the black contours; most of the wave patterns are not statistically significant on the surface, and only the Labrador Sea region has a significant signal. The new parameterization makes the surface water warmer in this region since the cold water is exported to the deep part of the ocean, consistent with the temperature anomalies at 2000 m depth. In the weak and moderate γ cases, there is a distinct cold plume all over the western part of the Atlantic. The t-test shows

that this cold water is a significant signal and it starts in the Labrador Sea and travels along the deep western boundary current (Fig. 8(d) and (f)). The eastern part of the South Atlantic Ocean and Southern Ocean has a positive warm anomaly. As expected, the Pacific Ocean at this depth is not affected by the new parameterization. There is a very strong cold anomaly at the surface and deep in the Labrador Sea for the $\gamma = 5$ case (Fig. 8(g) and (h)). However, the cold signal is not transported into the south unlike the other two weaker γ cases. To investigate the response at large γ further, horizontally averaged temperature is shown in Fig. 9. Horizontally averaged temperature for the control case in the Atlantic Ocean can be seen in Fig. 9(a). There is deep convected cold water at the Labrador Sea region (Lat $= 55°–60°$N). There is also evidence of Denmark Strait overflow water at Lat $= 65°$N. The temperature difference between control experiment and World Ocean Atlas climatology is shown in Fig. 9 (b). The convected water at the Labrador Sea is 0.5 degrees warmer than the climatological values. Fig. 9(c)–(f) depict the vertical section of the zonally averaged temperature difference between patchy sensitivity experiments and control simulation. For weak and moderate γ values, the upper ocean (i.e. depth < 1000 m) is warmer than the control simulation between 40°N and 60°N while the deep ocean gets colder in the same region, indicating that the patchy convection scheme increases the stratification in that area. However, the whole water column has a negative bias in the $\gamma = 5$ case. This barotropic signal does not travel to the south since there is a warm anomaly between 2000 and 3000 m depth south of 40°N.

Fig. 12. (a) Vertical section of the zonally averaged temperature difference between control experiment and climatology in the Southern Ocean; (b) Vertical section of the zonally averaged temperature difference between $\gamma = 0.15$ global eddy field and control experiment in the Southern Ocean; (c) same as (b) but for $\gamma = 0.5$; (d) same as (b) but for $\gamma = 1.25$. Note that the colorbars are different.

In summary, small or moderate values of γ increase stratification where the convection scheme is active. The cold water penetrates deeper and travels southward through the deep western boundary current. The results are not physical if we set γ as large as 5, possibly because the convected water is trapped at the bottom (as suggested by the extension of the mixed layer all the way to the bottom for large density differences in Fig. 3(d)) and unable to travel south in the deep boundary current. Thus, the next sequence of simulations, with realistic eddy velocities over the whole globe, will be performed only for γ values less than 5.

3.3. Global model results with prescribed EKE

In this section, three additional simulations have been performed using the prescribed eddy velocity field shown in Fig. 7(a) with $A = 0.5$. These experiments have different γ values which are $\gamma = 0.15, 0.5$ and 1.25. The results are described below.

The sea surface temperature difference between the $\gamma = 0.15$ and control experiments is shown in Fig. 10(a). As in the previous section, a wave-like pattern of cold and warm biases can be seen in the North Atlantic and Southern Oceans. These patterns are not statistically significant at 75%. In all prescribed EKE simulations, these wave patterns appear in the surface temperature biases but they are not significant. Increasing γ values only increases the amplitude of the patterns (Fig. 10(a), (c), (e)). Thus, we will not investigate surface temperature signals further. Fig. 10(b) shows the temperature difference at 2000 m depth for the $\gamma = 0.15$ case. The Labrador Sea is 0.2 °C colder at this depth.

The colder plume transported to the deep when patchy convection is used spreads through the western boundary current throughout the Atlantic Ocean. The same pattern is also visible for $\gamma = 0.5$ and $\gamma = 1.25$ (Fig. 10(d) and (f)). There is no significant signal in the Pacific Ocean. There are three likely reasons for that: (i) there are no deep-convection sites in the Northern Pacific; (ii) the EKE obtained from GM is negligible for most of the Pacific Ocean; (iii) the signal traveling from the deep North Atlantic did not reach the Pacific yet since the advective–diffusive time scale is probably larger than the model integration time. For the low and moderate γ values, the Southern Ocean cools at depth with the new parameterization.

The zonally-averaged temperature difference between the control experiment and World Ocean Atlas climatology values for the Atlantic and Southern Oceans (Fig. 11(a)) shows that there is a strong warm bias (almost 1–2 °C) in the Labrador Sea region (60°N). This warm bias is present throughout the whole deep Atlantic Ocean. In the $\gamma = 0.15$ case, the colder water is exported to the deep ocean around 60°N and spreads at 2000 m depth (blue shade in Fig. 11(b)). As a result, most of the deep Atlantic Ocean is slightly colder than the control case. The magnitude of temperature change is increased with increasing γ values. For $\gamma = 0.5$ and 1.25 experiments, the deep ocean is much cooler than the control case. Cooling the deep ocean improves the warm bias compared to the climatology. Note that the colorbars are different in Fig. 11. In the moderate γ case, the convected water is almost 0.25 °C colder in the Labrador Sea. Overall stratification in the North Atlantic is also increased with the patchy convection scheme.

The zonally-averaged temperature difference between control and climatology in the Southern Ocean is shown in Fig. 12(a). As for the Atlantic there is a strong warm bias in the deep Southern Ocean, especially on the shelf where the Antarctica Bottom Deep Water forms (south of 75°S). There is also a cold bias at the surface (above 100 m) and in the interior (between 250 m and 1800 m) south of 50°S while there is an approximately 150 m thick layer with a warm bias, between surface and interior waters. For the $\gamma = 0.15$ case, the surface water (100 m and above) bias is improved and the deep Southern Ocean is colder than the control case (Fig. 12(b)). Increasing γ also increases the magnitude of this temperature difference (Fig. 12(c) and (d)). Surface waters in the Southern Ocean are warmer than in the control case and there is a thick layer of colder water below it. The new parameterization also improves the warm bias on the Antarctic shelf where Lat $< 75°$S and depth < 800 m. However, the bias at intermediate depths is increased with the patchy convection scheme. We speculate that errors in the prescribed eddy kinetic energy field in the Southern Ocean may be responsible. For instance, if the eddy velocity field does not overlap with the convection sites, the patchy scheme will not perform well. Further investigation, which is beyond the scope of this paper, is required. In summary, the patchy convection scheme improves the overall biases and increases vertical stratification as expected. We also conclude that γ should be around 1.25 to see significant change in the mean state.

4. Discussion and conclusion

Ocean convection is a very important process for the large scale meridional overturning circulation in the ocean. All ocean general circulation models used in contemporary climate models have to parameterize this small scale phenomenon. In this study, we propose a new framework that can be used to represent convection in the open ocean as well as due to brine rejection under heterogeneous ice-cover. Details of the new scheme, which we term patchy convection, can be summarized as follows. The mean density profile can be decomposed into two profiles, and forcing and parameterized mixing due to heat loss or salt flux can be applied to the new profiles individually using existing schemes. Then, the decomposed profiles can be re-combined into the new mean state. The decomposition depends on two variables: the fractional area A of the unstratified density profile, and the density difference $\Delta\rho$ between unstratified and mean density profiles, which in turn can be estimated in terms of (i) eddy kinetic energy velocity, which can be estimated from the GM parameterization used in coarse resolution models, (ii) a nondimensional scaling coefficient γ. Using a single-column model, we first established that results are not very sensitive to the area fraction, and determined area fraction $A = 0.5$ to be a reasonable choice for all global tests. Then we tested the concept in a global ocean model with two different prescribed eddy velocity distributions and several different γ values.

In the first set of global experiments, we set the eddy velocity field to zero everywhere except the Labrador Sea region, ensuring that the patchy convection scheme was effective only in that region. We employed three different γ values: $\gamma = 0.5, \gamma = 1.25$ and $\gamma = 5$. The principal results are as follows: colder water was exported into the deep ocean in the North Atlantic and spread through the western boundary current; the stratification in the Labrador Sea region increased for $\gamma = 0.5$ and $\gamma = 1.25$ cases. The results of the $\gamma = 5$ experiment indicate that the patchy convection does not produce realistic values with very large γ values due to the nonlinear behavior of the scheme. For large γ, convection may reach too deep for the new watermass to exit the basin easily via the western boundary current. Next, we employed the realistic eddy velocity field around the globe with different γ values. Three

experiments are performed using $\gamma = 0.15, 1$ and 1.25. The results indicate that the patchy convection scheme improves the warm biases in the deep Atlantic Ocean and Southern Ocean. The vertical stratification is increased compared to the control case. In the Labrador Sea, 0.2 °C cold water is exported into the deep ocean with the new convection scheme, a significant improvement compared to the control, since the bias from climatology is around 1 °C. However, other factors not addressed here could also contribute to this bias. The reductions in bias seen here are similar to those noted when the representation of overflows is improved (Danabasoglu et al., 2010). Both model improvements tend to increase the supply of dense cold water at depth. Given that both open ocean convection and overflows contribute to the North Atlantic Deep Water, both improvements will be needed for more accurate modeling of North Atlantic climate and its variability.

In this preliminary investigation we have not attempted to develop a theory for γ, the scaling factor. More accurate determination of the relationship between the GM bolus velocity and the eddy density anomaly would be required, and we leave this to future work.

In conclusion, the new framework scheme proposed here can be used to improve parameterization of convection in coarse resolution global simulations. In the future, the patchy convection scheme could be improved by using a prognostic eddy velocity field (Eden and Greatbatch, 2008). For instance, Marshall and Adcroft (2010) describe a new mesoscale eddy closure scheme which has a prognostic eddy kinetic energy field. In addition, the new scheme could be used to parameterize heterogeneous convection due to under-ice brine rejection processes. The numerical implementation is straight forward, and the computational cost is minimal.

Acknowledgement

References

Aagaard, K., Carmack, E.C., 1989. The role of sea ice and other fresh water in the Arctic circulation. J. Geophys. Res. 94, 14485–14498.

Boccaletti, G., Ferrari, R., Fox-Kemper, B., 2007. Mixed layer instabilities and restratification. J. Phys. Oceanogr. 37, 22–28.

Campin, J.-M., Hill, C., Jones, H., Marshall, J., 2011. Super-parameterization in ocean modeling: application to deep convection. Ocean Model. 36, 90–101.

Cessi, P., 2008. An energy-constrained parameterization of eddy buoyancy flux. J. Phys. Oceanogr. 38, 1807.

Chelton, D.B., Deszoeke, R.A., Schlax, M.G., El Naggar, K., Siwertz, N., 1998. Geographical variability of the first baroclinic Rossby radius of deformation. J. Phys. Oceanogr. 28, 433–460.

Cox, M.D., 1984. A primitive equation, three-dimensional model of the ocean. GFDl Ocean Group Tech. Rep. 1, GFDL-Princeton University.

Danabasoglu, G., Large, W.G., Briegleb, B.P., 2010. Climate impacts of parameterized Nordic Sea overflows. J. Geophys. Res. (Oceans) 115, 11005.

Demirov, E.K., Pinardi, N., 2007. On the relationship between the water mass pathways and eddy variability in the Western Mediterranean Sea. J. Geophys. Res. (Oceans) 112, 2024.

Dickson, R.R., Gmitrowics, E.M., Watson, A.J., 1990. Deep water renewal in the northern north atlantic. Nature 344, 848–850.

Dunne, J.P., John, J.G., Adcroft, A.J., Griffies, S.M., Hallberg, R.W., Shevliakova, E., Stouffer, R.J., Cooke, W., Dunne, K.A., Harrison, M.J., Krasting, J.P., Malyshev, S.L., Milly, P.C.D., Phillipps, P.J., Sentman, L.T., Samuels, B.L., Spelman, M.J., Winton, M., Wittenberg, A.T., Zadeh, N., 2012. GFDL's ESM2 global coupled climate-carbon earth system models. Part I: physical formulation and baseline simulation characteristics. J. Clim. 25, 6646–6665.

Eden, C., Greatbatch, R.J., 2008. Diapycnal mixing by meso-scale eddies. Ocean Model. 23, 113–120.

Fox-Kemper, B., Ferrari, R., Hallberg, R., 2008. Parameterization of mixed layer eddies. Part I: theory and diagnosis. J. Phys. Oceanogr. 38, 1145.

Gascard, J.-C., Watson, A.J., Messias, M.-J., Olsson, K.A., Johannessen, T., Simonsen, K., 2002. Long-lived vortices as a mode of deep ventilation in the Greenland Sea. Nature 416, 525–527.

Gelderloos, R., Katsman, C.A., Drijfhout, S.S., 2011. Assessing the roles of three eddy types in restratifying the Labrador Sea after deep convection. J. Phys. Oceanogr. 41, 2102–2119.

Griffies, S.M., 2012. Elements of the Modular Ocean Model (MOM): 2012 release (GFDL Ocean Group Technical Report No. 7). NOAA/Geophysical Fluid Dynamics Laboratory, Princeton, USA, 614 + xiii pages.

Griffies, S.M., Biastoch, A., Böning, C., Bryan, F., Danabasoglu, G., Chassignet, E.P., England, M.H., Gerdes, R., Haak, H., Hallberg, R.W., Hazeleger, W., Jungclaus, J., Large, W.G., Madec, G., Pirani, A., Samuels, B.L., Scheinert, M., Gupta, A.S., Severijns, C.A., Simmons, H.L., Treguier, A.M., Winton, M., Yeager, S., Yin, J., 2009. Coordinated ocean-ice reference experiments (COREs). Ocean Model. 26, 1–46.

Griffies, S.M., Gnanadesikan, A., Dixon, K.W., Dunne, J.P., Gerdes, R., Harrison, M.J., Rosati, A., Russell, J.L., Samuels, B.L., Spelman, M.J., Winton, M., Zhang, R., 2005. Formulation of an ocean model for global climate simulations. Ocean Sci. 1, 45–79.

Ilcak, M., Özgökmen, T.M., Peters, H., Baumert, H.Z., Iskandarini, M., 2008. Performance of two-equation turbulence closures in three-dimensional simulations of the Red Sea overflow. Ocean Model. 24, 122–139.

Jones, H., Marshall, J., 1997. Restratification after deep convection. J. Phys. Oceanogr. 27, 2276–2287.

Katsman, C.A., Spall, M.A., Pickart, R.S., 2004. Boundary current eddies and their role in the restratification of the Labrador Sea. J. Phys. Oceanogr. 34, 1967.

Klinger, B.A., Marshall, J., Send, U., 1996. Representation of convective plumes by vertical adjustment. J. Geophys. Res. 101, 18175–18182.

Large, W.G., McWilliams, J.C., Doney, S.C., 1994. Oceanic vertical mixing: a review and a model with a nonlocal boundary layer parameterization. Rev. Geophys. 32, 363–403.

Legg, S., McWilliams, J., Gao, J., 1998. Localization of deep ocean convection by a mesoscale eddy. J. Phys. Oceanogr. 28, 944–970.

Lilly, J.M., Rhines, P.B., 2002. Coherent eddies in the labrador sea observed from a mooring. J. Phys. Oceanogr. 32, 585–598.

Lilly, J.M., Rhines, P.B., Schott, F., Lavender, K., Lazier, J., Send, U., D'Asaro, E., 2003. Observations of the Labrador Sea eddy field review article. Prog. Oceanogr. 59, 75–176.

Losch, M., Herlufsen, S., Timmermann, R., 2006. Effects of heterogeneous surface boundary conditions on parameterized oceanic deep convection. Ocean Model. 13, 156–165.

Marshall, D.P., Adcroft, A.J., 2010. Parameterization of ocean eddies: potential vorticity mixing, energetics and Arnold's first stability theorem. Ocean Model. 32, 188–204.

Marshall, J., Schott, F., 1999. Open-ocean convection: observations, theory, and models. Rev. Geophys. 37, 1–64.

Nguyen, A.T., Menemenlis, D., Kwok, R., 2009. Improved modeling of the Arctic halocline with a subgrid-scale brine rejection parameterization. J. Geophys. Res. (Oceans) 114, 11014.

Paluszkiewicz, T., Romea, R.D., 1997. A one-dimensional model for the parameterization of deep convection in the ocean. Dyn. Atmos. Oceans 26, 95–130.

Rahmstorf, S., 1993. A fast and complete convection scheme for ocean models. Ocean Model. 101, 9–11.

Rhein, M., Coauthors, 2002. Labrador sea water: pathways, CFC inventory, and formation rates. J. Phys. Oceanogr 32, 648–665.

Rykova, T., Straneo, F., Lilly, J.M., Yashayaev, I., 2009. Irminger current anticyclones in the Labrador Sea observed in the hydrographic record, 1990–2004. J. Marine Res. 67, 361–384.

Schott, F., Leaman, K.D., 1991. Observations with moored acoustic Doppler current profilers in the convection Regime in the Golfe du Lion. J. Phys. Oceanogr. 21, 558–574.

Smethie, W., Fine, R.A., 2001. Rates of North Atlantic deep water formation calculated from chlorofluorocarbon inventories. Deep Sea Res. Part I: Oceanographic Res. 48, 189–215.

Smith, S.D., Muench, R.D., Pease, C.H., 1990. Polynyas and leads: an overview of physical processes and environment. J. Geophys. Res. 95, 9461–9479.

Spall, M.A., 2004. Boundary currents and watermass transformation in marginal seas. J. Phys. Oceanogr. 34, 1197.

Straneo, F., 2006. On the Connection between dense water formation, overturning, and poleward heat transport in a convective basin*. J. Phys. Oceanogr. 36, 1822.

Våge, K., Pickart, R.S., Moore, G.W.K., Ribergaard, M.H., 2008. Winter mixed layer development in the central Irminger Sea: the effect of strong, intermittent wind events. J. Phys. Oceanogr. 38, 541.

Våge, K., Pickart, R.S., Sarafanov, A., Knutsen, Ø, Mercier, H., Lherminier, P., van Aken, H.M., Meincke, J., Quadfasel, D., Bacon, S., 2011. The Irminger Gyre: circulation, convection, and interannual variability. Deep Sea Res. Part I: Oceanographic Res. 58, 590–614.